NANO: Brief Reports and Reviews
Vol. 10, No. 7 (2015) 1550096 (12 pages)

DOI: 10.1142/S1793292015500964

Study of Biomolecules Imaging Using Molecular Dynamics Simulations

Mohsen Kheirodin*, Hossein Nejat Pishkenari†,
Ali Moosavi‡ and Ali Meghdari§
School of Mechanical Engineering
Sharif University of Technology, Tehran, Iran
**kheirodin@mech.sharif.edu*
†*nejat@sharif.edu*
‡*moosavi@sharif.edu*
§*meghdari@sharif.edu*

Received 26 March 2015
Accepted 18 May 2015
Published 10 July 2015

The process of imaging a biomolecule by atomic force microscope (AFM) is modeled using molecular dynamics (MD) simulations. Since the large normal force exerted by the tip on the biosample in contact and tapping modes may damage the sample structure and produce irreversible deformation, the noncontact mode of AFM (NC-AFM) is employed as the operating mode. The biosample is scanned using a carbon nanotube (CNT) as the AFM probe. CNTs because of their small diameter, high aspect ratio and high mechanical resistance attract many attentions for imaging purposes. The tip–sample interaction is simulated by the MD method. The protein, which has been considered as the biomolecule, is ubiquitin and a graphene sheet is used as the substrate. The effects of CNT's geometric parameters such as the CNT height, the diameter, the tilt angle, the flexibility and the number of layers on the image quality have been evaluated.

Keywords: AFM; biosample imaging; molecular dynamics simulation; CNT geometry.

1. Introduction

Due to its capability of imaging biosamples both in air and liquid at nanometer resolution, atomic force microscope (AFM) has been evolved into a powerful tool in the detection of extremely small and soft biological materials. The contact mode has rarely been used for biosample imaging because it can damage the biomolecule structure by applying a large repulsive force, which leads to plastic deformation of the biosample.[1] Although the tapping mode of AFM (TM-AFM) reduces the applied force on the sample surface compared to the contact mode, it cannot be used in imaging the soft biological samples. Some repulsive interaction forces applied on the biosample, although fewer in comparison with the contact mode, may affect the vulnerable structure of the biomolecule. Noncontact mode of AFM (NC-AFM) does not suffer from the sample degradation effects, making it preferable for measuring soft samples such as biological samples and organic thin films. This operation mode is unable to provide information on the mechanical

†Corresponding author.

properties of the sample due to elimination of the repulsive tip–sample contact. Since in our study, we attempt to image a vulnerable protein, we will use the NC mode.

As mentioned before, we will consider CNT as the AFM probe. CNTs have been widely used for AFM imaging and manipulation.[2–14] There are certain properties of CNTs that make them ideal tips for AFMs compared to silicon or diamond tips including the ability to be fabricated with a small diameter ranging between approximately 1–2 nm and 0.4 nm,[8] high elastic modulus, high aspect ratio and good chemical properties. Their high elastic modulus provides a high mechanical resistance which helps in avoiding fracture and reducing thermal vibration effects even in small diameters.[7] Their large aspect ratio makes them suitable for imaging a sample which has large aspect ratio too.

In spite of the significant role of tip geometry on the direct interaction with surface and imaging resolution, only a few papers have been devoted to the study of the geometry of the tip on imaging quality. For instance, Nejat and Meghdari[15] investigated the effects of tip geometry on Amplitude Modulation AFM (AM-AFM) images using MD simulations. Their results demonstrate when the sample feature is sharper than the tip, the image is dominated by the shape of the tip. In another research,[16] they investigated the influence of the system part flexibilities on the TM-AFM measurements using MD simulations. They found that independent of the amplitude setting, when the sample flexibility increases, the tip and substrate deformation and also the interaction force decrease. Furthermore, they realized that if the sample stiffness is small with respect to the stiffness of the tip and the substrate (for most practical samples such as biological samples), then the deformations of the substrate and the tip are small with respect to the sample deformation.

There are just a few works that have evaluated the properties of CNTs on the image quality. For example, Solares *et al.*[11] investigated the effect of tilt angle on the imaging process of a particle with multi-walled carbon nanotubes (MWNTs) with about 3.5 nm diameter. They also evaluated the effect of elastic deformation of single walled carbon nanotubes (SWNTs) on the imaging from a rigid nanoparticle.[10]

The main goal of our research is to evaluate the effect of geometric parameters of SWNTs with a diameter of about 0.5–1.5 nm on the sequent image quality, then subsequently investigating the effectiveness of using double walled carbon nanotubes (DWNTs) or MWNT. Although due to their small diameter, it seems that SWNTs are more suitable for imaging a small biosample with respect to MWNT, their lower stiffness may affect the image quality (as we will see).[5]

The method which is used here to obtain the tip–sample interaction force versus the tip height diagram (F–z diagram) is molecular dynamics (MD). Nowadays MD is becoming a very powerful tool for modeling dynamic behaviors of nanodevices such as AFM in imaging or manipulation processes. For example the modeling of the positioning process of a nanoparticle with AFM,[17] imaging with AFM by Nejat *et al.*[15,18–21] and Solares *et al.*,[11,22] scratching of a solid surface with AFM,[23–25] plastic deformation of a biomolecule in indentation process[26] and extension a biosample with AFM[27–29] have been performed by MD simulations to understand atomic scale behavior. In this study, we use steered molecular dynamics (SMD), a feature of NAMD software, for modeling the imaging process. The next section explains the setup and the implementation steps.

2. The Proposed System

In this section, we will explain the simulation setup prepared for imaging of a biomolecule in the NC mode. An AFM tip consists of two parts, the silicon cone and CNT which is located on the apex of the silicon part. The substrate is a graphite sheet, but for simplification in the MD simulations, we assume a graphene sheet as a substrate and calculate and add the long-range attractive force between the silicon part of the tip and the bulk section of the graphite substrate according to Eq. (1), which refers to the van der Waals interaction force between a cone and a sheet.[30]

$$F_{\text{flat surface–sphere}} = \frac{A_H R}{6D^2}, \tag{1}$$

where D stands for the nearest distance between the cone and sheet, $A_H = 29.6 \times 10^{-20}$ J represents the graphite-silicon Hamaker constant[31] and $R = 5$ nm is the sphere radius. Thus, in the MD simulations we only consider the CNT and the graphene sheet as the substrate and finally add up the interaction force from Eq. (1) and the MD simulation [see Fig. 1].

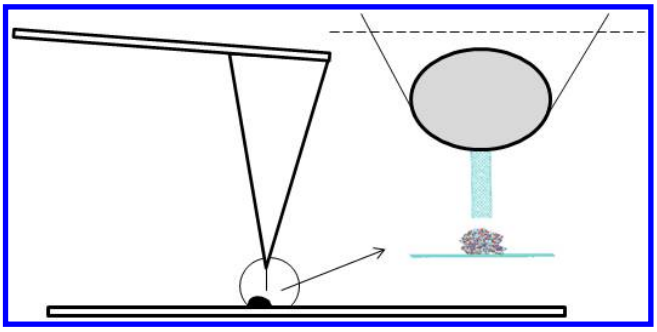

Fig. 1. Silicon section of tip and graphite sheet interaction calculated by long-range van der Waals relation.

We used Ubiquitin as the biomolecule, a flexible biosample which can be surrounded by a cube of 34 Å length. This protein can be found in approximately all tissues of eukaryotic organisms. This protein binds to other proteins and labels them for destruction. The ubiquitin protein is composed of 76 amino acids including 1231 atoms. Before using the biosample in our simulation, it is relaxed and minimized in a water box for 0.1 ns. Figure 2 shows the Ubiquitin after minimization and equilibration. Also it should be mentioned that after merging the system elements together, they are minimized and relaxed for 0.1 ns.

To reduce the biosample flexibility effect, we have rotated it until the most flexible part is located at the bottom of the protein. In order to prevent the lateral sliding of the protein during the approach of the tip, 24 of its atoms closest to the surface were kept fixed. The MD setup has been illustrated in Fig. 3.

We intend to take a NC-AFM image of the Ubiquitin. In this regard, the tip–sample vertical interaction force is calculated using MD. For this purpose, the tip approaches to the sample vertically at a fixed horizontal position with a constant speed, while recording the interaction force between the tip and the surface. We want to scan a cross section of the protein along the x-axis.

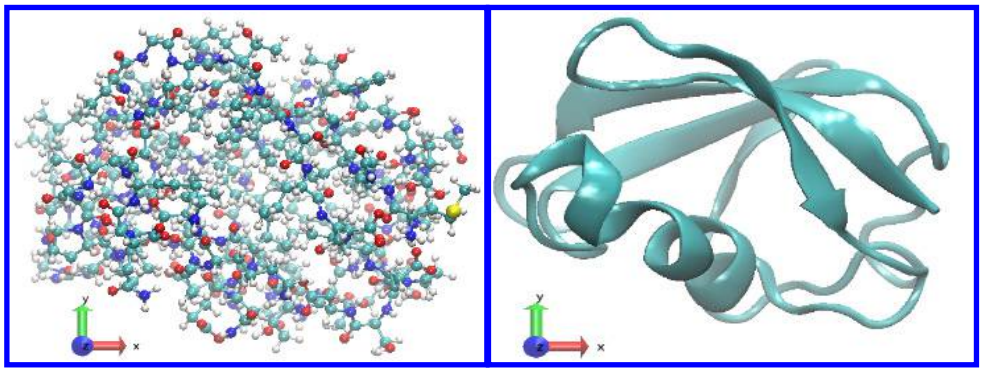

(a) (b)

Fig. 2. CPK (a) and New-cartoon (b) modes representation of Ubiquitin minimization and equilibration.

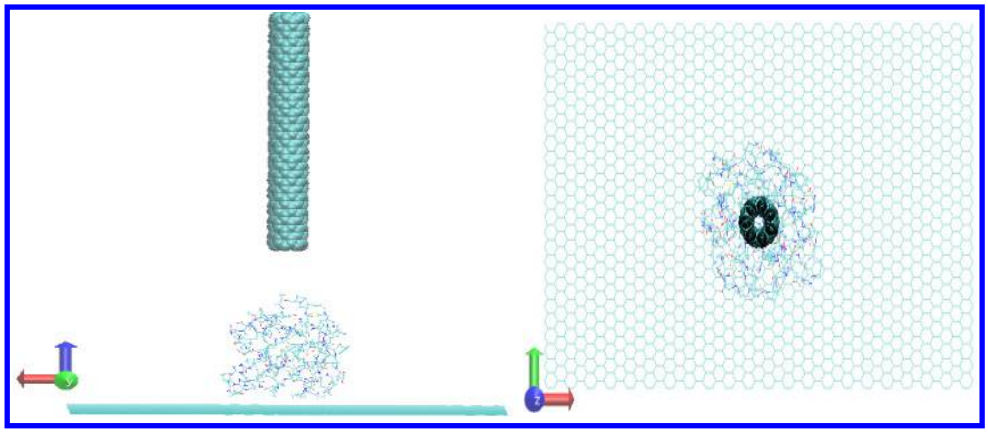

Fig. 3. The prepared MD setup in horizontal and vertical views with the CNT tip, graphene as substrate and Ubiquitin as biosample.

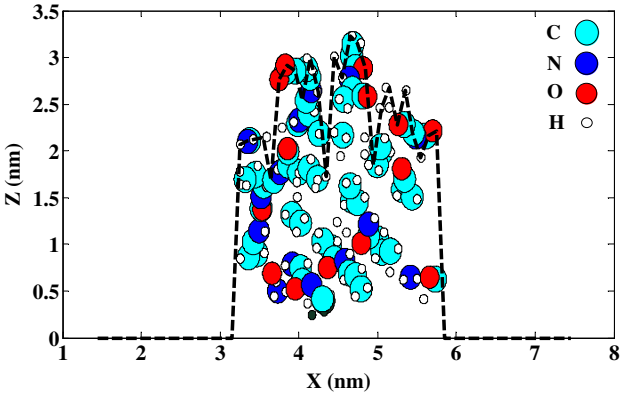

Fig. 4. Selected cross section of the biosample and substrate which will be scanned by AFM probe. The selected cross section is divided to 61 points with an equal distance 1 Å.The horizontal position of points −30 and 61 are $x = 1.5$ nm and 7.5 nm, respectively. The protein atoms depicted in figure are those atoms having a distance less than 2 Å from the selected cross section.

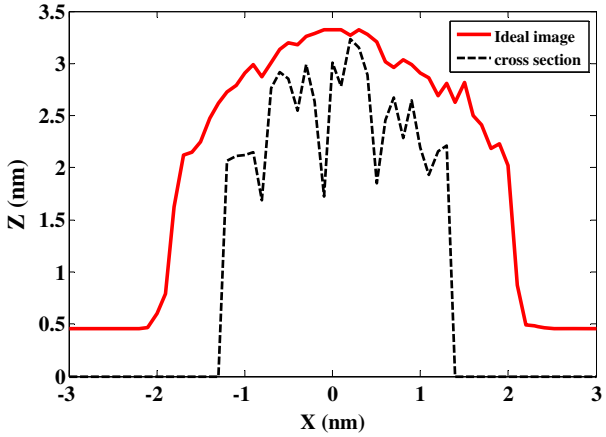

Fig. 5. The image of the biosample with ideal tip, the best theoretical image with CNTs in NC mode (color online).

In Fig. 4, the selected realistic cross section of the protein is depicted. We divided the cross section into 61 horizontal points with an equal distance of 1 Å. Points −30 and 61 belong to $x = 1.5$ nm and $x = 7.5$ nm, respectively. Then, we use MD to obtain for each horizontal point. In order to produce an image from the surface, we calculate the interaction force versus the image height (using Eq. (5) in Sec. 3) at these 61 points.

It is worthy to note that a realistic cross section cannot be captured due to several practical reasons. First of all, the geometry of the tip superimposes itself on the raw scan data measured from the specimen. In addition, due to flexibility of the tip, the substrate and the sample, the tip–sample interaction force induces system deformation. Generally speaking, the elastic deformation of the system elements leads to the particle height lowering in the measured topography. Furthermore, NC mode imaging restricts the tip movement to the attractive region of the tip–sample interaction diagram. Thus, the tip position and the sequent topography are about 3–4 Å above the sample. Moreover, the variety of biosample atoms and different neighbor atoms of the cross section may influence the topography.

The best image from a sample can be taken by a very sharp (small diameter and high aspect ratio) tip having a high stiffness (low flexibility). In order to compare our images with this ideal image, we assume a virtual CNT tip which is rigid and has a very small diameter as the ideal tip. Then, we obtain the biosample's cross section topography with this tip as an ideal image. Ideal CNT is assumed to have a 3.9 Å diameter, an infinity length and a rigid structure. Figure 5 shows the biosample topography (red curve) with an ideal tip.

To move the tip above the biosample, we use the SMD method, which makes it possible to apply a constant force to a number of atoms or move them with constant velocity. This method has been widely used in recent years for evaluating the dynamics behavior between the AFM tip and the sample in different applications[27–29,32,33] In this study, we use the constant velocity SMD. In this method, the NAMD software moves selected atoms with specified velocity.[33] As we choose higher spring stiffness, the constant velocity approximation for SMD atoms will improve.

We select 1 nm top atoms of the CNT as SMD and constrained atoms, which are forced to move only in the Z-direction with the SMD velocity of 1 m/s. Because of the multi-scale property of the system, simulating the tip movement with its real velocity is very time consuming. Thus, we should find an optimized velocity which does not affect the dynamic behavior of the system. To this end, we have conducted several simulations by halving the tip velocity value and observing when the simulation results do not change considerably. Here, we have calculated the interaction force between the tip and the sample for different velocities using MD. Figure 6 depicts the (F–z) diagram for three tips with vertical velocities of 0.5 m/s, 1 m/s and 2 m/s. As can be seen in Fig. 6, the interaction force between the tip and the protein behavior does not change significantly near the velocity of 1 m/s.

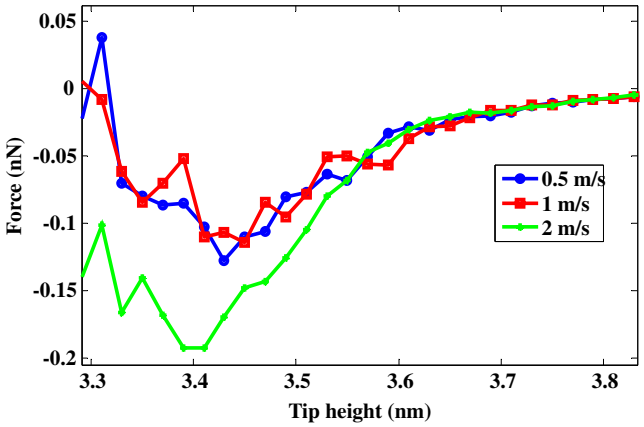

Fig. 6. Interaction force versus tip movement for different tip velocities, the behavior does not change in velocities below 1 m/s.

Thus, we choose 1 m/s as a suitable speed for the tip movement.

The biomolecule after minimization and relaxation in a periodic water box, is added to the main setup. To prevent the biomolecule's instability and to simply model the environment, we have employed Langevin dynamics (LD). Although considering the solvent media implicitly cannot model the effect of CNT hydrophobicity, LD method is able to mimic many effects of the environment by considering effects such as random and frictional forces on the biomolecule atoms with lower computational cost. Other MD simulation parameters are presented in Table 1. In our simulations, CNT atoms are supposed to be neutral, and it should be noted that this assumption may not be true generally and depends on the termination and functionalization process of the CNT.

Since the calculated F–z diagram has some undesirable fluctuations, we use a fitting function to remove them. The fitting function used here is:

$$F = \begin{cases} -\exp(a_1 z^2 + b_1 z + c_1) & z > z_{c1} \quad (2a) \\ a_2 z + b_2 & z_{c2} < z < z_{c1} \quad (2b) \\ a_3 z^2 + b_3 z + c_3 & z < z_{c2} \quad (2c) \end{cases}$$

Table 1. MD simulation parameters.

Variable	Description
Temperature	300 K
Thermostat	Langevin dynamics
Time step	2 femto's, Rigid bonds
Boundary Condition	Graphene atoms are rigid
Cut off distance	12 Ă
Pair-list distance	13.5 Ă

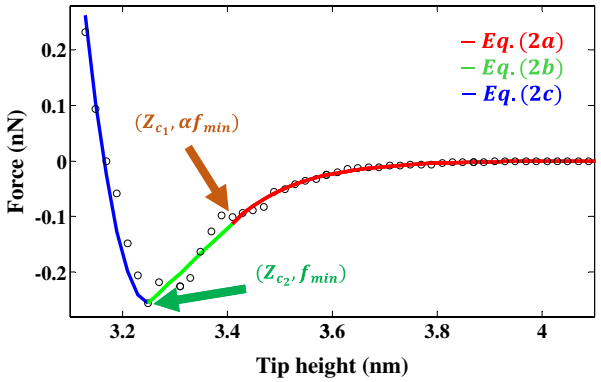

Fig. 7. Tip–sample interaction force curve for the system in point 0 ($x = 4.5$ nm). The small circles give the MD force values and the solid lines correspond to Eq. (2). The proposed fitting function are defined for three different regions.

where z_{c2} is the tip's height corresponding to minimum force ($f_{\min}$) and z_{c1} is the tip's height for $\alpha f_{\min}$, where the coefficient $\alpha \in (0.1)$ decreases as the CNT's flexibility increases. Other coefficients are obtained from the continuity of the F–z diagram and the least square method. The difference between the proposed fitting function and that of Solares *et al.*[22] are in dividing the ascending attractive region into two parts, and using the exponential function for the first part. Dividing the first section into two subparts is necessary especially for CNTs with high flexibility which produce a (F–z) diagram that varies a lot along the ascending attractive region. Figure 7 shows the fitness quality of the proposed function at the middle point of the biosample.

Figure 8 shows the schematic lumped model of AFM cantilever in vertical excitation (VE) imaging modes.

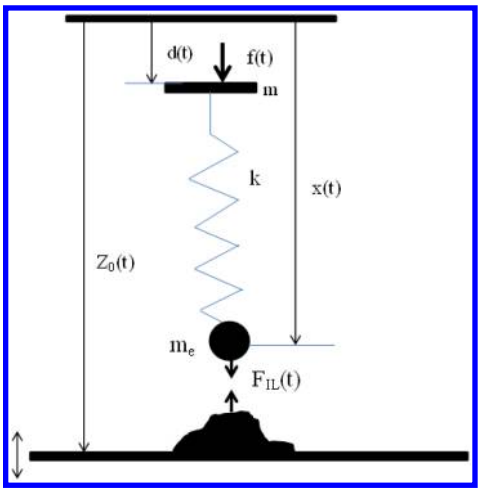

Fig. 8. Lumped model of AFM.

Table 2. The vibration's parameters.

A, Amplitude	11 nm
k, Stiffness	2 N/m
$f0$, Resonance frequency	200 kHz
Desired frequency shift	40 z

The dynamic equations of the tip motion are[34]:

$$m\ddot{d}(t) + b(\dot{d}(t) - \dot{x}(t)) + k(d(t) - x(t)) = f(t), \quad (3)$$

$$m_e\ddot{x}(t) + b(\dot{x}(t) - \dot{d}(t)) + k(x(t) - d(t) = f_{IL}(t)), \quad (4)$$

where $f(t)$ is the piezo actuator force applied to the cantilever $f_{\text{in}}(t)$ and is the tip–sample interaction force. Here, for NC mode imaging we can use two PI controllers to maintain the vibration amplitude and frequency shift at the desired values by tuning $f(t)$ and the substrate height, respectively. Assuming perfect performance of frequency and amplitude controllers, the frequency shift for each vibration cycle is given as:

$$\Delta f(d, k, A, f_{IL}) = -\frac{f_0}{2\pi kA}\int_0^{2\pi} f_{\text{in}}(d + A + A\cos(\phi))d\phi, \quad (5)$$

where A is the oscillation amplitude and k represents the cantilever stiffness. Because of small interaction force between the tip and the sample, the vibration resonance frequency should be large and k and A (amplitude) should be small to have a reasonable magnitude of frequency shifts. On the other hand, to improve the image resolution, we should set the frequency shift at maximum value within stable imaging region. We have chosen an optimized magnitude of frequency shift of 40 Hz for our imaging simulations. The utilized parameters in our simulations are presented in Table 2.

3. Results

As mentioned before, to reproduce the realistic images of the biosample, we should use two different PI controllers to maintain the vibration amplitude and frequency shift at the desired values. However, in our next simulations, we will try to measure ideal images, which can be obtained by using Eq. (5) assuming the controllers are working perfectly. In order to compare the images obtained from these two techniques, i.e., the perfect controller and real controller, we have produced the biosample topography by these methods. Figure 9 depicts the effect of scanning velocity on the image quality. An examination of the figure reveals that increasing the scanning velocity reduces the image quality.

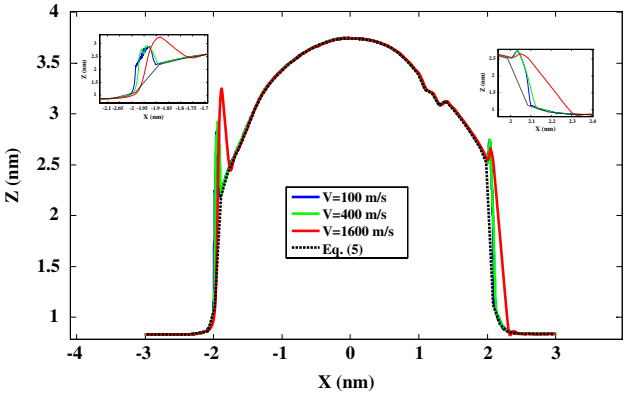

Fig. 9. The effect of the scanning velocity on the image quality, as the scanning velociy increases, the overshoot of the measured topography with respect to ideal image increases.

In the next sections, we attempt to investigate the effects of the different CNT parameters on the quality of the produced topography.

3.1. *CNT's diameter*

One of the most important geometric parameters of CNTs is their diameter. Using SWNTs makes it possible to have tips with diameters of about 1–2 nm. While Hafner *et al.*,[3] and Woolley *et al.*[4] have indicated that the minimum diameter of SWNT is about 0.7 nm, Chen *et al.*[8] have reported the CNT diameter to be 0.4 nm.[8] Generally speaking, increasing the CNT diameter leads to low flexibility, which is desirable; but because of the tip broadening effect, it reduces the image quality. In the present study, we have chosen CNT diameters to be $D1 = 5.4$ Å, $D2 = 8.1$ Å, $D3 = 10.9$ Å and $D4 = 14.1$ Å with a length of $L1 = 50$ Å. The tip broadening effect for different CNTs is depicted in Fig. 11. The measured topography illustrated in Fig. 11 are obtained assuming that all of the system elements are rigid. This assumption help us to distinct the effects of the tip broadening from the effects of the tip flexibility (Fig. 12). From the results shown in Fig. 10, it may be concluded that the tip broadening effect can be easily calibrated.

Figure 11 shows the biosample topography for the real flexible tip and biosample. Results indicate that as the tip diameters increases the image's

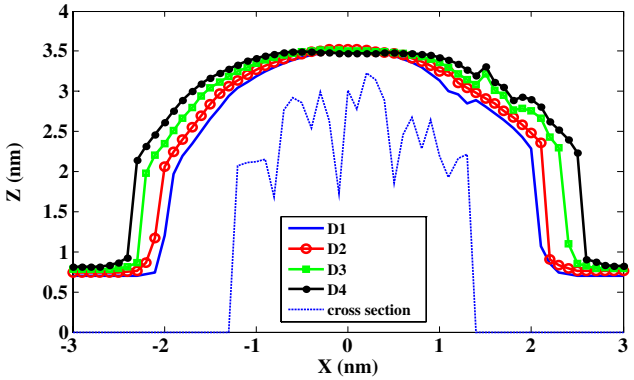

Fig. 10. The tip broadening effect. The image becomes broader as the CNT diameter increases. In this simulation, the system elements are assumed to be rigid.

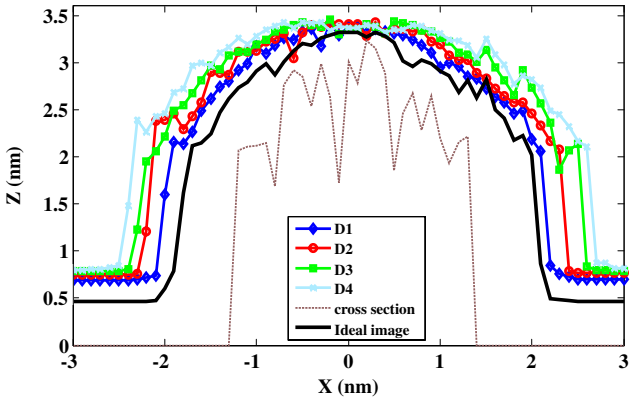

Fig. 11. The effect of the tip diameter on the image quality. In this simulation, all the system elements are assumed to be flexible.

quality improves due to the smaller tip flexibility, but this effect is less than the tip broadening effect. The effect of tip's length and flexibility will be investigated more in the next section. As we mentioned previously, the ideal image shown in Fig. 5 is the image taken by a rigid CNT with a diameter $D1 = 3.9\,\text{Å}$ having an infinity length. As is evident in Fig. 11 the measured images are wider than the ideal image because of the tip broadening effect and their flexibility. Furthermore, the infinity length of the ideal image leads to zero force between the silicon part of the tip and the graphite. Thus, the ideal image is below the other images.

3.2. *CNT's length*

It is expected that if the CNT length increases the image quality decreases, due to more tip deflection. The effect of CNT length on its flexibility and

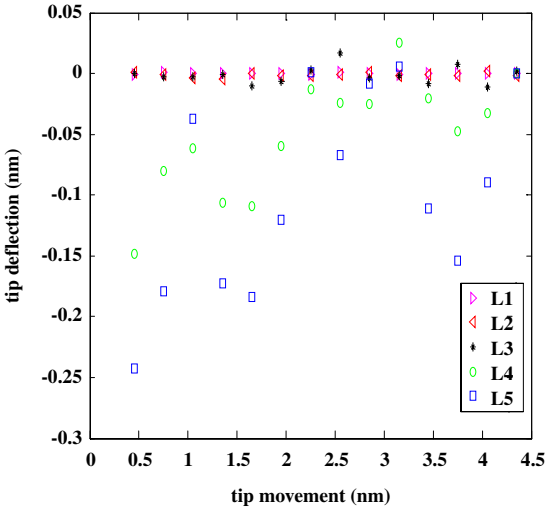

(a)

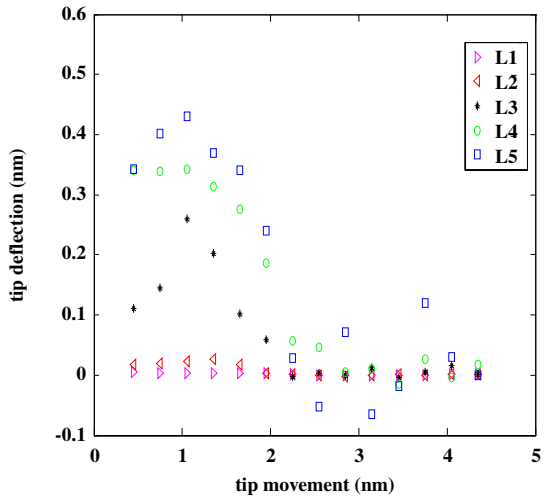

(b)

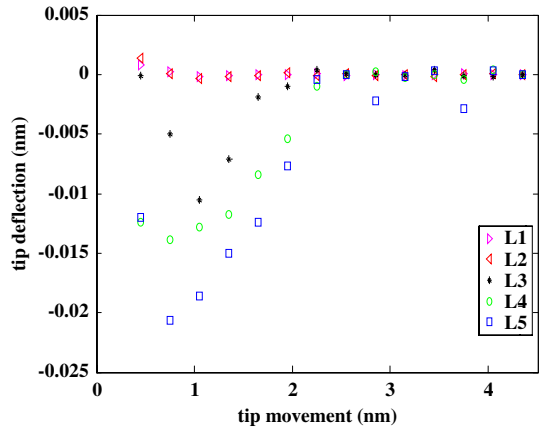

(c)

Fig. 12. The effect of CNT's length on its deflection in x (part (a)), y (part (b)) and z (part (c)) directions. As the CNT length increases its deformation increases too.

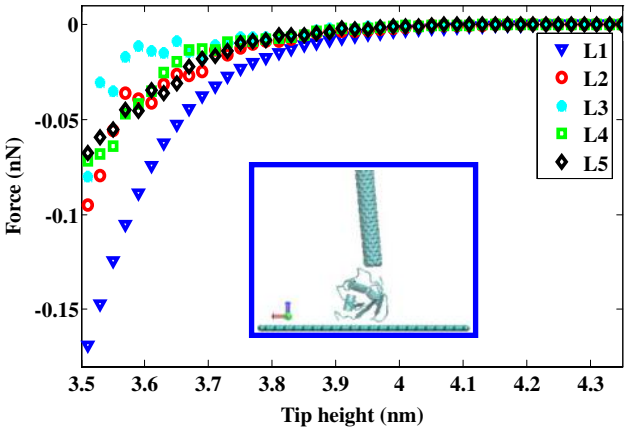

Fig. 13. The effect of CNT's length on F–z diagram, point +1 (middle).

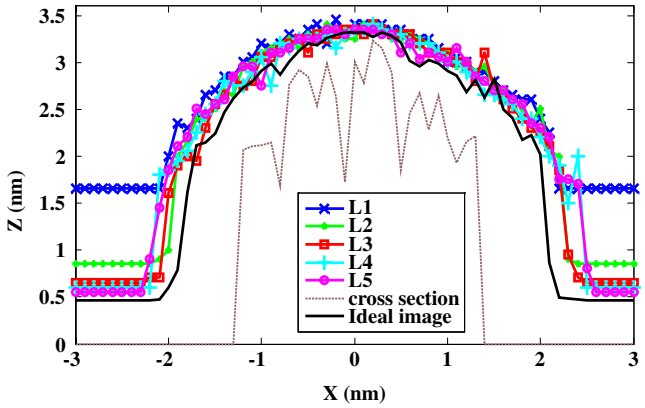

Fig. 15. The effect of CNT's length on image's quality for $D = D1$, higher length cause to more fluctuations in image and lower long range attractive force.

deflection has been illustrated in Fig. 12, showing the tip deflection in different directions (for point +1). The CNT lengths are assumed to be $L1 = 30\,\text{Å}$, $L2 = 40\,\text{Å}$, $L3 = 50\,\text{Å}$, $L4 = 60\,\text{Å}$ and $L5 = 70\,\text{Å}$ with a diameter of $D1 = 5.4\,\text{Å}$. Intentionally the tip's diameter is considered to be small to demonstrate the CNT flexibility effects more evidently.

The effect of CNT length on the interaction force for a middle point and an edge point of the biosample is depicted in Figs. 13 and 14.

The CNTs shown in Figs. 13 and 14 indicate the considerable tip deflection due to interaction forces between tip and sample. Therefore, it is reasonable to conclude that images taken by longer CNTs have more topographical irregularities than the images of short CNTs. Figure 15 shows the effect of CNT's length on the biosample topography and it is obvious that as the CNT's length increases the image's quality decreases, in particular for the edge points.

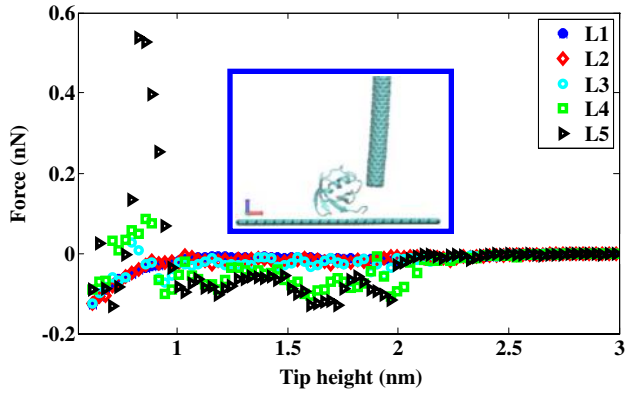

Fig. 14. The effect of CNT's length on F–z diagram, point +22 (edge).

As mentioned before, as the CNT length decreases the distance between the silicon part of the AFM tip and the substrate decreases. In fact, in these conditions the van der Waals part of the interaction force, between the silicon part of the AFM tip and the substrate, has a substantial role on the total force exerted on CNT. This force, between the bulk parts of the tip and the substrate, reduces the effects of the local interaction forces, between atomic parts of the tip and the sample, on the measured topography leading to a lower image resolution. When the CNT length increases, the bulk forces between the tip and the substrate reduces and to produce the desired frequency shift the tip should approach closer to the substrate. This effect is obvious in Figs. 15 and 16. Since the ideal tip has an

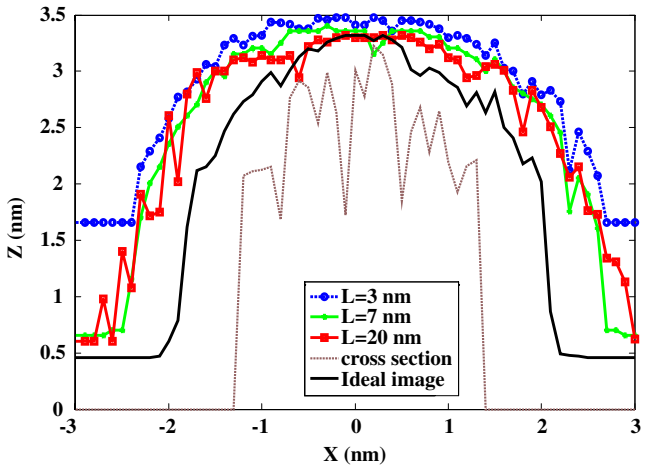

Fig. 16. The effect of CNT's length on image's quality for $D = D5$, in this case fluctuations appear in length of 20 nm because of higher CNT diameter.

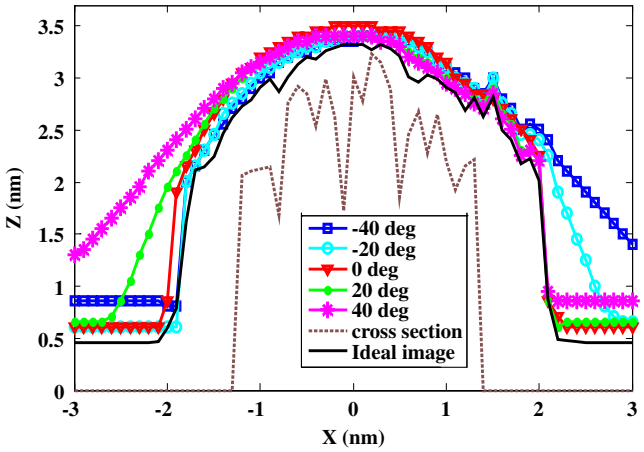

Fig. 17. The the effect of tilt angle on biosample's image, atoms are considered rigid, this error despite of tip broadening cannot be calibrated.

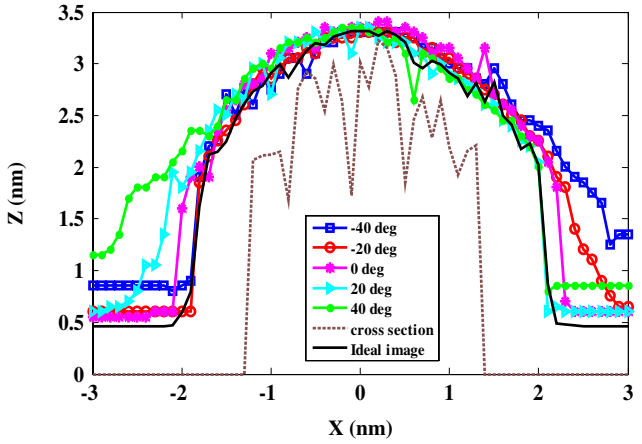

Fig. 18. The effect of CNT's x-direction tilt on image's quality.

infinity length, the image taken by this tip is below the other images.

Now we examine the CNT length effect for a larger diameter $D5 = 12.51\,\text{Å}$. As expected, the results indicate that the CNT flexibility exposes its effect on the images quality at larger lengths. Here we examine the CNT lengths of $L1 = 30\,\text{Å}$, $L5 = 70\,\text{Å}$ and $L6 = 200\,\text{Å}$. As is illustrated in Fig. 16, the image corruption, because of CNT higher flexibility at higher lengths, occurs at $L6 = 200\,\text{Å}$ and not at $L5 = 70\,\text{Å}$.

3.3. *CNT's tilt angle*

One of the imaging artifacts, which may create problems in the imaging, arises from the probe tilt angle. Here, we examine the effects of CNT tilt angles in the x-direction (perpendicular to scanning direction) and y-directions on sequent images. The tilt angles were supposed to be $+20°$, $+40°$, $-20°$ and $-40°$ in the x-direction and $+20°$ and $+40°$ in the y-direction. The first effect is that because of tip apex deviation, the tip–sample interaction is influenced by the neighboring atoms of the sample rather than the desired atoms (atoms placed exactly below the CNT), this effect can be named "shape effect of the CNT tilt" and can be seen obviously in Fig. 17, whose images are achieved with rigid atoms assumption. Unfortunately, despite the tip broadening effect, this shape effect error cannot be calibrated. The difference between the measured and the ideal image increases with increasing the tilt angle. The second problem is that the CNT tilt causes a bending force along the CNT, which leads to the tip deflection. Solares *et al.*[11] investigated the mechanical effects of tilt angle in SWNT and MWNT tips during tapping mode imaging from a rigid nanoparticle.

Figure 18, which shows the effect of tilt angle on the image quality with MD simulations, expresses that this effect is negligible compared to the shape effect. The CNTs have a diameter of $D1 = 5.4\,\text{Å}$ and a length of $L3 = 50\,\text{Å}$.

3.4. *CNT's flexibility*

The purpose of this section is the comparison between the effect of the CNT and biosample flexibility on the measured topography of the biosample. Generally speaking, as the CNT aspect ratio decreases or number of its layers increases, the influence of CNT flexibility increases. Shapiro *et al.*[10] studied the effect of SWNT and sample deformation during the imaging process. Here, we compare the flexibility effect between a CNT with diameter $D1 = 5.4\,\text{Å}$ and length of $L3 = 50\,\text{Å}$ and ubiquitin as the biosample. First, we obtain the image assuming that all of the system elements are flexible. Second, we consider the biosample atoms rigid. Third, consider just the CNT atoms rigid and finally consider the whole setup atoms rigid and compare the obtained topographies from the four mentioned conditions. Figures 19 and 20 show the comparison of (F–z) diagrams for the four conditions for a middle point and an edge point of the biosample.

As we expected the trend of F–z diagrams for both edge and middle points are similar to the (F–z)

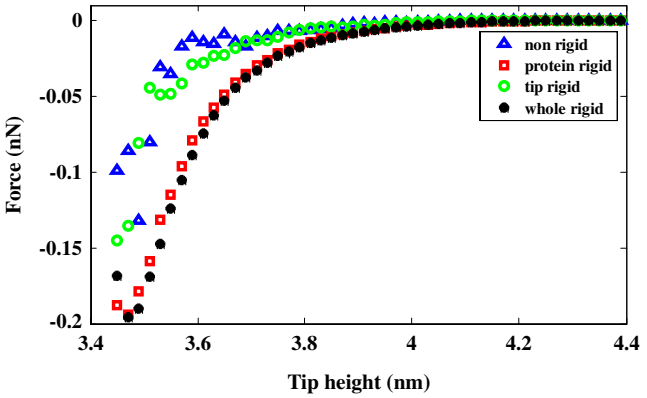

Fig. 19. The effect of CNT's and biosample's on F–z diagram, point +1 (middle), the trends are like the F–z diagram for different lengths.

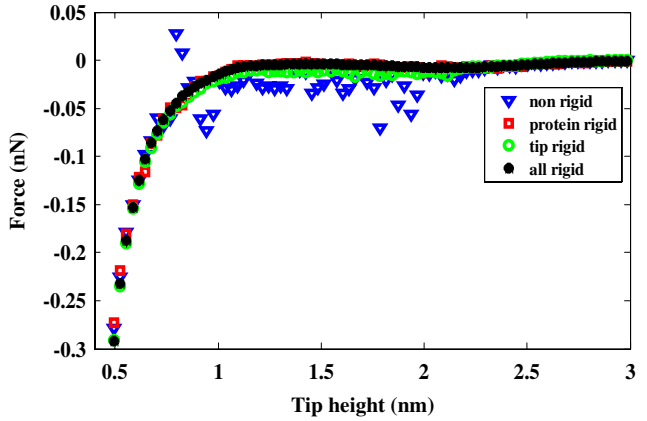

Fig. 20. The effect of CNT's and biosample's on F–z diagram, point +22 (edge), the trends are like the F–z diagram for different lengths.

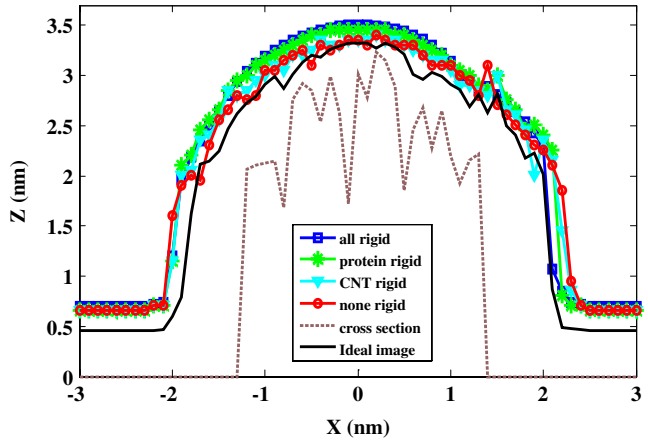

Fig. 21. The effect of CNT's and biosample's flexibility on image's quality, the sample flexibly has the greatest role in image corruption.

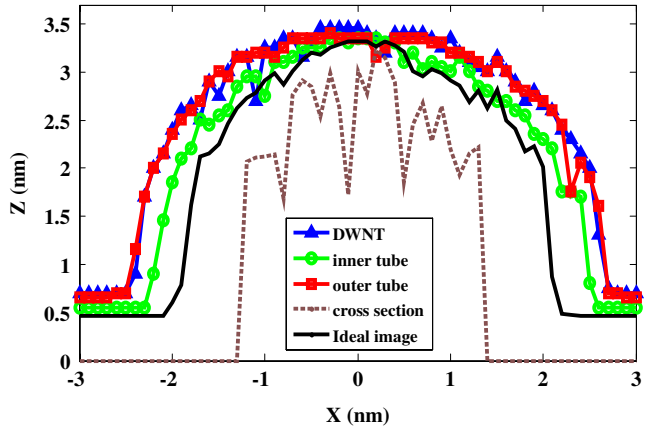

Fig. 22. Comparison between the obtained image with SWNT and DWNT, outer tube and DWNT have about the same images for $L = 7$ nm.

diagrams for different lengths (Figs. 13 and 14). Figure 21 shows the obtained topographies. It can be concluded that the effect of biosample flexibility is more than the effect of CNT flexibility and this is especially obvious for edge points.

3.5. *MWNTs or SWNTs*

It is expected that SWNTs, because of their lower possible diameters, are more suitable for molecule scale imaging than MWNTs. On the other hand, DWNTs may improve imaging quality in some cases because of their mechanical stiffness is more compared to SWNTs.[4] Here we consider two SWNT tips with diameters of 5.4 Å and 15.2 Å and length 70 Å. Also we use a DWNT with inner diameter of 5.4 Å, outer diameter of 15.2 Å, and length 70 Å. In manufacturing MWNTs, the gap distance between the tubes must be at least 3.4 Å.[4]

It is worthy to note that, two SWNT tips are the same as inner and outer tubes of DWNT tip, respectively. We name the small SWNT as inner tube, and the large SWNT as outer tube. Figure 22 depicts the image taken by two SWNT tips and DWNT tip. It is obvious that the image taken by the inner tube is more accurate than the ones taken by the outer tube and DWNT. However, the DWNT and outer tube calibrated images will be more accurate because of their lower aspect ratio and flexibility.

As it is shown in Fig. 22, the measured topography of the outer tube (SWNT) and DWNT are

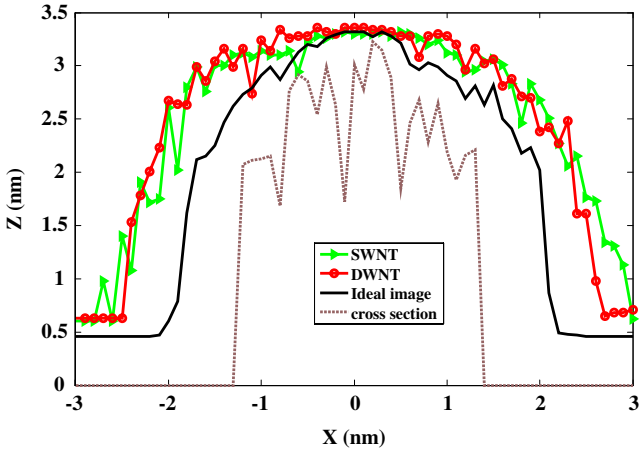

Fig. 23. The image of a monolayer and a double layer CNT with $L = L6$, for length of 20 nm the higher mechanical resistance of DW shows itself.

approximately similar. To study the role of the tip length on the image taken by these tips, we have increased the tips length from 70 Å to 200 Å. Figure 23 illustrates the images taken by two SWNT tips as well as the image taken by DWNT tip. As it is demonstrated in this figure, the image of DWNT is more precise than the images taken by SWNTs. The images of SWNTs have more fluctuations particularly in the edge points of the sample in comparison with the image of DWNT and this is due to additional flexibility of the SWNT tips.

To examine the stiffness of the mentioned tips, here we have compared the flexibility of the larger SWNT with the flexibility of DWNT. For this purpose, we have fixed one side of the CNTs and applied a constant force $F = 0.2$ nN perpendicularly on the tip of CNT. The results indicate that the stiffness of the DWNT tip is about 10% more than the stiffness of the SWNT. This is the reason why the DWNT image has less fluctuations compared to the SWNTs images.

4. Conclusion

Characterization of the nanoscale biosamples with high spatial resolution, is an essential technology for the study of biological materials. In this paper, we presented the simulation of biosample imaging by NC-AFM. The results provide an important physical insight, which reveals the significant role of the different parameters such as the diameter, length, number of layers (DW or SW) and tilt angle of the tip on NC-AFM measurements. Some of the main conclusions demonstrating the effects of the tip parameters on NC-AFM measurements are as follows:

It has been demonstrated that some of parameters such as the tilt angle, diameter and length of the tip affect the imaging quality significantly while the other parameters such as the number of layers of the tip and the scan speed have a little effect on the measured topography.

Independent of the frequency shift set-point, the images taken in the NC-AFM mode with the assumption of a rigid tip and sample is above the image of the flexible realistic system, and the difference between these two images increases in more flexible parts of the sample.

The size of the CNT diameter has two effects on the image quality. First, the tip broadening caused by the tip's shape and, the second, the effect of flexibility. The effect of the tip broadening can be calibrated easily, and the flexibility at a length less than 50 Å has a little effect on the image quality. We examined CNTs with different lengths of 30 Å to 70 Å. Results revealed that as the CNT length increases the image quality decreases, particularly in the edge points. Of course this effect is negligible for larger diameters in this range of length. For instance, the results demonstrate that for a CNT with the diameter of $D = 12.5$ Å, the CNT length only influences the image quality of L200 Å.

Similar to the tip diameter, the tip tilt angle has two effects on image quality: a mechanical effect and a shape effect. In our scales, the mechanical effects are negligible compared to the shape effects. Furthermore, despite the tip broadening effect which is the shape effect due to the nonzero CNT diameter, the shape effect of CNT tilt angle on achieved images cannot be calibrated.

Although, DWNTs are stiffer than SWNTs, this issue has a small effect on the image quality when CNT length is lower than 10 nm (aspect ratio of about 4–5). But, DWNTs exhibit more stiffness and lower deflections when CNT length exceeds 20 nm, where the image of SWNTs has too fluctuations and errors, especially in the edge points.

A series of simulations have been conducted to compare the effect of the biosample flexibility on the measured topography with the effect of the CNT flexibility on it. The results showed that although the examined CNT ($D = 5.4$ Å and aspect ratio of 10) is too flexible, the flexibility of biosample plays a more important role on the resultant image.

Acknowledgment

The authors would like to thank the Iranian National Science Foundation (INSF) for their financial support.

References

1. Y. L. Lyubchenko, *Micron* **42**, 196 (2011).
2. H. Takahashi, S. Numao, S. Bandow and S. Iijima, *Chem. Phys. Lett.* **418**, 535 (2006).
3. J. H. Hafner, C. L. Cheung, A. T. Woolley and C. M. Lieber, *Prog. Biophys. Mol. Biol.* **77**, 73 (2001).
4. A. T. Woolley, C. L. Cheung, J. H. Hafner and C. M. Lieber, *Chem. Biol.* **7**, 193 (2000).
5. C. Lamprecht, J. Danzberger, P. Lukanov, C. M. Tilmaciu, A. M. Galibert, B. Soula, E. Flahaut, H. J. Gruber, P. Hinterdorfer, A. Ebner and F. Kienberger, *Ultramicroscopy* **109**, 899 (2009).
6. J. H. Lee, W. S. Kang, B. S. Choi, S. W. Choi and J. H. Kim, *Ultramicroscopy* **108**, 1163 (2008).
7. Y. Wang and X. Chen, *Ultramicroscopy* **107**, 293 (2007).
8. L. Chen, C. L. Cheung, P. D. Ashby and C. M. Lieber, *Nano Lett.* **4**, 1725 (2009).
9. N. Choi, T. Uchihashi, H. Nishijima, T. Ishida, W. Mizutani, S. Akita, Y. Nakayama, M. Ishikawa and H. Tokumoto, *Jpn. J. Appl. Phys.* **39**, 3707 (2009).
10. I. R. Shapiro, S. D. Solares, M. J. Esplandiu, L. A. Wade, W. A. Goddard and C. P. Collier, *J. Phys. Chem. B* **108**, 13613 (2004).
11. S. D. Solares, Y. Matsuda and W. A. Goddard, *J. Phys. Chem. B* **109**, 16658 (2005).
12. K. Kostarelos, A. Bianco and M. Prato, *Nat. Nanotechnol.* **4**, 627 (2009).
13. N. R. Wilson and J. V. Macpherson, *Nat. Nanotechnol.* **4**, 483 (2009).
14. X. Zongwei, F. Fang and S. Dong, *Carbon Nanotube AFM Probe Technology* (INTECH Open Access Publisher, 2011).
15. H. N. Pishkenari and A. Meghdari, *Ultramicroscopy* **111**, 1423 (2011).
16. H. N. Pishkenari and A. Meghdari, *Micro Nano Lett. IET.* **6**, 1023 (2011).
17. S. H. Mahboobi, A. Meghdari, N. Jalili and F. Amiri, *Curr. Appl. Phys.* **9**, 997 (2009).
18. H. N. Pishkenari, S. H. Mahboobi and A. Meghdari, *J. Phys. D: Appl. Phys.* **44**, 75303 (2011).
19. H. N. Pishkenari and A. Meghdari, *Curr. Appl. Phys.* **10**, 583 (2010).
20. H. N. Pishkenari and A. Meghdari, *Ultramicroscopy* **111**, 107 (2011).
21. H. N. Pishkenari, S. H. Mahboobi and A. Meghdari, *Micro Nano Lett.* **6**, 412 (2011).
22. S. D. Solares and J. C. Crone, *J. Phys. Chem. C* **111**, 10029 (2007).
23. J. J. Zhang, T. Sun, Y. D. Yan, Y. C. Liang and S. Dong, *Appl. Surf. Sci.* **254**, 4774 (2008).
24. J. Zhang, T. Sun, Y. Yan and Y. Liang, *Mater. Sci. Eng.* **505**, 65 (2009).
25. P. Z. Zhua, Y. Hu, H. Wanga and T. B. Maa, *Mater. Sci. Eng. A* **528**, 4522 (2011).
26. A. Arkhipov, W. H. Roos, G. J. L. Wuite and K. Schulten, *Biophys. J.* **97**, 2061 (2009).
27. S. B. Fowler, R. B. Best, J. L. T. Herrera, T. J. Rutherford, A. Steward, E. Paci, M. Karplus and J. Clarke, *J. Mol. Biol.* **322**, 841 (2002).
28. I. M. Neelov, D. B. Aldof, T. C. B. McLeish and E. Paci, *Biophys. J.* **91**, 3579 (2006).
29. M. Hamdi, A. Ferreira, G. Sharma and C. Mavroidis, *Microelectron J.* **39**, 190 (2008).
30. H.-J. Butt, B. Cappella and M. Kappl, *Surf. Sci. Rep.* **59**, 1 (2005).
31. A. Delnavaz, *Curr. Appl. Phys.* **10**, 1416 (2010).
32. K. Masugata, A. Ikai and S. Okazaki, *Appl. Surf. Sci.* **188**, 372 (2002).
33. J. C. Phillips, R. Braun, W. Wang, J. Gumbart, E. Tajkhorshid, E. Villa, C. Chipot, R. D. Skeel, L. Kale and K. Schulten, *J. Comput. Chem.* **26**, 1781 (2005).
34. H. N. Pishkenari, M. Behzad and A. Meghdari, *Chaos Solitons Fractals* **37**, 748 (2008).